Contents lists available at ScienceDirect

Food and Bioproducts Processing

journal homepage: www.elsevier.com/locate/fbp

Computational fluid dynamics combined with discrete element method and discrete phase model for studying a food hydrofluidization system

*Jesica D. Oroná, Susana E. Zorrilla, Juan M. Peralta**

Instituto de Desarrollo Tecnológico para la Industria Química (INTEC), Universidad Nacional del Litoral—CONICET, Güemes 3450, S3000GLN Santa Fe, Argentina

ARTICLE INFO

Article history:
Received 9 July 2016
Received in revised form 8 November 2016
Accepted 11 January 2017
Available online 19 January 2017

Keywords:
Hydrofluidization
DEM
DPM
CFD
Food
Mathematical modeling
Freezing

ABSTRACT

A food hydrofluidization system composed by multiple fluid immersed jets and multiple moving food spheres was modeled using computational fluid dynamics (CFD) coupled with discrete element method (DEM) and discrete phase model (DPM). The model proposed consists in studying the fluid and food domains separately and connecting both through the information carries by surface heat transfer coefficients. The fluid flow was solved considering Navier–Stokes assumptions for a Newtonian fluid, the movement of food spheres was followed by DPM while the interactions of spheres between them and with the wall domain were considered through DEM. Specific parameters were determined for a study case of potato spheres when a concentrated NaCl solution was used as refrigerating medium. The proposed model was partially validated with information obtained from literature for similar systems and good agreement was found. This study shows, as a proof of concept, that CFD–DPM–DEM can be a powerful tool to simulate food processing systems where particles of food solid move within the fluid domain with a minimum computational requirement.

1. Introduction

Hydrofluidization (HF) is a relatively novel technique for chilling and freezing that uses a refrigerating liquid that is pumped upwards to form immersed liquid jets and a fluidized bed of highly turbulent liquid with moving products (Fikiin, 1992; Fikiin and Fikiin, 1998). This technology brings together the advantages of both air fluidization and immersion food freezing techniques. Some of the benefits associated with HF are (Fikiin and Fikiin, 1998; Fikiin, 2003, 2008): high heat transfer rates with small temperature gradients, fine ice crystal structure in foods, small size of equipment, relatively easy operation, products individually frozen and an environmentally friendly process. It is easy to note that, based on these features, HF is a substantial improvement and intensification (Stankiewicz and Moulijn, 2004) over traditional freezing techniques.

Different contributions to the process modeling have been developed recently (Verboven et al., 2003; Peralta et al., 2007, 2009, 2010, 2012; Belis et al., 2015). The physical situation of heat and mass transfer between food and fluid combined with food pieces to be frozen moving around the fluid domain was conveniently faced from simple configurations (*i.e.* single static sphere and single jet) to more complex ones (*i.e.* several static spheres and multiple jets). Taking into account mobile foods is the next step in this progressive approach to represent the physical scenario of HF.

The fluid-particles systems are rather complex to represent theoretically, computational fluid dynamics (CFD) being a tool of choice due to sustained and significant advances in model fidelity, computational hardware and algorithms (Wu et al., 2014). A simple strategy for modeling multiphase flows is the combination of CFD with discrete phase model (DPM) and discrete element method (DEM). In DPM, the fluid phase is considered a continuum by solving the Navier–Stokes equations, while the dispersed phase is solved by tracking the particles through the calculated flow field. DEM completes the information related to particle–particle interactions by the so-called "soft sphere"

* *Corresponding author*. Fax: +54 342 451 1079.
E-mail address: jmperalta@intec.unl.edu.ar (J.M. Peralta).
http://dx.doi.org/10.1016/j.fbp.2017.01.005

Nomenclature

A_y	Cross sectional area to the domain axis at the height y [m^2]
C_D	Drag coefficient [–]
C_{NaCl}	Volume-averaged NaCl concentration in the potato spheres [$g\,kg^{-1}$]
Cp	Fluid heat capacity [$J\,kg^{-1}\,K^{-1}$]
D	Diameter of the spheres [cm]
d	Diameter of the orifices [cm]
$\langle d_t \rangle$	Dimensionless average minimum distance defined by Eq. (26) [–]
$\underline{e}$	Unit vector between two spheres [–]
F_D	Drag force per unit sphere mass [$m\,s^{-2}$]
$\underline{F}_{DEM}$	Force per unit sphere mass due to the interactions between spheres estimated by DEM [$m\,s^{-2}$]
$\underline{F}_N$	Normal component of $\underline{F}_{DEM}$ [$m\,s^{-2}$]
$\underline{F}_T$	Tangential component of $\underline{F}_{DEM}$ [$m\,s^{-2}$]
f_{loss}	Loss factor [–]
$\underline{g}$	Gravity acceleration vector [$m\,s^{-2}$]
H_0	Initial position of spheres relative to the orifice plate [mm]
h_c	Surface heat transfer coefficient [$W\,m^{-2}\,K^{-1}$]
h_c^*	Averaged surface heat transfer coefficient obtained by Belis et al. (2015) [$W\,m^{-2}\,K^{-1}$]
h_0, h_1, h_2	Distances used in the determination of the coefficient of restitution [m]
$\langle h_c \rangle$	Volume-averaged surface heat transfer coefficient defined by Eq. (24) [$W\,m^{-2}\,K^{-1}$]
$\langle\langle h_c \rangle\rangle$	Time-averaged $\langle h_c \rangle$ defined by Eq. (25) [$W\,m^{-2}\,K^{-1}$]
K	Spring constant per unit mass [s^{-2}]
k	Fluid thermal conductivity [$W\,m^{-1}\,K^{-1}$]
k_c	Mass transfer coefficient [$m\,s^{-1}$]
L	Initial minimum distance among the geometric centers of the spheres [cm]
m	Mass [kg]
Nu_D	Nusselt number based on D (h_cD/k) [–]
Pr	Prandtl number ($Cp\mu/k$) [–]
R	Radius [m]
Re_D	Reynolds number based on D and v_{slip} ($\rho D v_{slip}/\mu$) [–]
r	Radial position [m]
$\underline{r}$	Position vector [m]
S	Minimum distance among the geometric centers of the orifices [cm]
s_{limit}	Parameter determining how fast μ approaches μ_{limit} [$s\,m^{-1}$]
T	Temperature [°C]
T_c	Temperature of the geometric center of the spheres [°C]
t	Time [s]
t_0	Initial time [s]
t_{coll}	Collision time scale [s]
t_f	Final time [s]
t_{Res}	Total residence time of the spheres in the domain [s]
Tu	Local turbulence intensity ($\sqrt{2/3\kappa}/\lvert\underline{v}_f\rvert$) [–]
$\langle Tu \rangle$	Volume-averaged Tu defined by Eq. (23) [–]
V	Volume [m^3]
V_o	Area averaged fluid velocity at the orifices [$m\,s^{-1}$]
V_T	Volume of the fluid domain [m^3]
$\underline{v}$	Fluid velocity vector [$m\,s^{-1}$]
v_{glide}	Gliding velocity [$m\,s^{-1}$]
v_{slip}	Magnitude of $\underline{v}_p - \underline{v}_f$ [$m\,s^{-1}$]
v_{limit}	Limit velocity [$m\,s^{-1}$]
$\langle v_f \rangle$	Area-averaged $\lvert\underline{v}_f\rvert$ at A_y [$m\,s^{-1}$]
$\langle v_p \rangle$	Volume-averaged $\lvert\underline{v}_p\rvert$ defined by Eq. (21) [$m\,s^{-1}$]
$\langle v_{slip} \rangle$	Volume-averaged v_{slip} defined by Eq. (22) [$m\,s^{-1}$]
y	Axial position in the fluid domain [m]

Greek symbols

γ	Damping coefficient [s^{-1}]
δ	Overlap between the spheres p and p' [–]
η	Coefficient of restitution [–]
κ	Turbulence kinetic energy [$m^2\,s^{-2}$]
μ	Viscosity [Pa s]
$\mu_{friction}$	Friction coefficient [–]
μ_{glide}	Gliding friction coefficient [–]
μ_{limit}	High velocity limit friction coefficient [–]
μ_{stick}	Sticking friction coefficient [–]
ρ	Density [$kg\,m^{-3}$]
ω	Specific turbulence dissipation rate [s^{-1}]

Subscripts

f	Fluid
p	Sphere p or sphere-sphere interactions
$p-p'$	Relative between spheres p and p'
T	Tangential
w	Sphere–wall interactions

Acronyms

CFD	Computational fluid dynamics
DEM	Discrete element method
DPM	Discrete phase method

approach (Cundall and Strack, 1979; Fluent, 2011). The soft sphere approach (Cundall and Strack, 1979) is a simplified model that assumes that the influence of the particle of interest is limited only to neighboring particles which are in direct contact by allowing a slight overlap (Crowe et al., 2012; Wu, 2012). The interactions are modeled as a dynamic process where contact forces accumulate or dissipate over time and can be calculated through the deformation history at the contact (Wu, 2012).

Studies related to granular materials combining CFD with DEM appeared in the literature in the early 1990's (Thornton, 2015), while food applications for similar systems were first reported a decade later (Norton and Sun, 2007; Fryer et al., 2011; Norton and Tiwari, 2014). Some combinations of CFD, DEM and DPM have been proposed using self-developed code, and commercial (*e.g.* CFX, Fluent) and open source (*e.g.* OpenFoam) CFD tools to describe the heat and mass transfer (and its intensification) in fluidized beds, suspensions and solid-liquid mixing of foods (Norton and Sun, 2007; Fries et al., 2011; Fryer et al., 2011; Kloss et al., 2012; Ren et al., 2012; Norton and Tiwari, 2014; Tsotsas and Mujumdar, 2014; Zhang et al., 2014). Although, some extrapolation of those results can be made to HF, the nature of the material (*i.e.* phase-change food samples) and the refrigerating medium (*i.e.* liquid) used in

HF gives sufficient room for new proposals and studies of the transport phenomena in HF combining CFD with DEM and DPM.

The objective of this work was to use, as a proof of concept, a coupling between CFD, DPM and DEM to describe the transport phenomena involved in a hydrofluidization system with moving food spheres and multiple round jets and to complete the formulation with the necessary parameters.

2. Materials and methods

2.1. System studied

The studied hydrofluidization system consisted in a cylindrical vessel of 100-mm diameter and 100-mm in height and a plate with 3-mm diameter round orifices to produce 69 jets at its base (Fig. 1). A regularly spaced squared array of 10-mm diameter spheres (13 spheres) initially placed at a distance H_0 of 30 mm from the orifice plate was used. The spheres were considered made by potato (*Solanum tuberosum* L.) to model the heat and mass transfer in a food sample. An aqueous solution of NaCl was considered to model the refrigerating medium (with a concentration of 0.231 kg kg^{-1} (w/w)) and the occluded solution in the food sample. A refrigerating medium temperature $T = -5\,^{\circ}C$ and an area averaged fluid velocity at the orifices $V_o = 1.18\,m\,s^{-1}$ were also considered.

2.2. Mathematical modeling of the transport phenomena involved in the system studied

The mathematical modeling of the transport phenomena of the system proposed in this study solved for each time step: (a) the heat, mass and momentum transfer in the liquid refrigerating medium by combining CFD with DPM and DEM, and then, (b) the heat and mass transfer inside the food sample using a validated mathematical model. The information of the first step was used to estimate the velocity (and position) of the particles through DPM and DEM (i.e. soft sphere model). An average surface heat transfer coefficient for each sphere was obtained and it was used to transfer information from the liquid to the solid phase. The second step consisted in solving a heat and mass transfer model proposed in previous studies

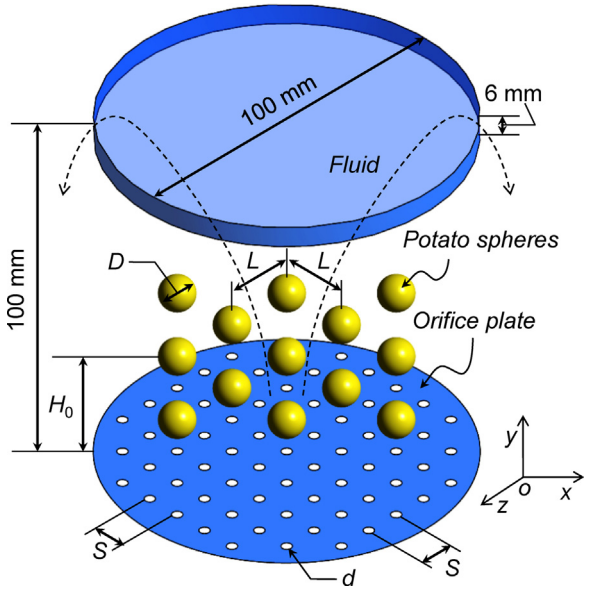

Fig. 1 – Schematic diagram of the hydrofluidization system studied.

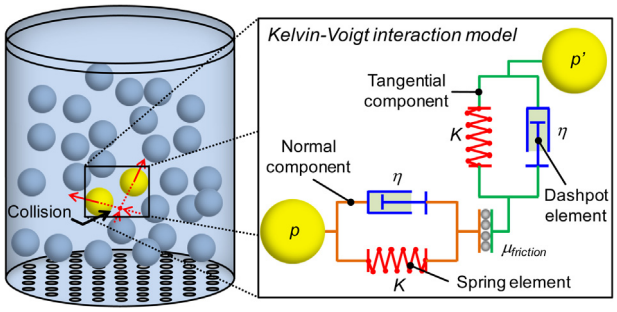

Fig. 2 – Schematic diagram of the Kelvin–Voigt model for interactions between spheres.

(Zorrilla and Rubiolo, 2005a,b; Peralta et al., 2010, 2012) assuming that transport phenomena mainly occurred in the radial direction.

It is worthwhile to mention that even though the mathematical model can be easily used with a large amount of particles (Crowe et al., 2012), only 13 spheres were used to simplify this presentation.

2.2.1. Heat, mass and momentum transfer in the liquid refrigerating medium

The momentum (Navier–Stokes) and mass (continuity) balances in the liquid refrigerating medium domain for a hydrofluidization system were solved by CFD and assuming that the fluid is Newtonian. The turbulence phenomenon was taken into account by using the two parameter model $\kappa-\omega$ Shear Stress Transport (SST) (Wilcox, 2006).

DPM allows estimating the velocity vector of a sphere p ($\underline{v}_p$) as (Fluent, 2011; Crowe et al., 2012; Schulze et al., 2014):

$$\frac{d\underline{v}_p}{dt} = F_D\left(\underline{v}_f - \underline{v}_p\right) + \frac{(\rho_p - \rho)}{\rho_p}\underline{g} + \underline{F}_{DEM} \quad (1)$$

where $\underline{v}_f$ is the local fluid velocity, ρ_p is the density of the sphere p, ρ is the fluid density, $\underline{g}$ is the gravity acceleration vector, $\underline{F}_{DEM}$ is the force per unit sphere mass due to the interactions between spheres estimated by DEM and F_D is the drag force per unit sphere mass estimated by (Gidaspow, 1994):

$$F_D = \frac{18\mu}{\rho_p D^2}\frac{C_D Re_D}{24} \quad (2)$$

where μ is the fluid viscosity, D is the diameter of sphere p, C_D is the drag coefficient and Re_D is the Reynolds number based on the diameter of sphere p and on the magnitude of the relative particle local velocity to the fluid local velocity ($\rho D v_{slip}/\mu$). The drag coefficient was estimated with Wen–Yu model that was suggested for systems where the solid phase volume is less than the 20% of the total volume, where the drag coefficient is estimated as (Gidaspow, 1994; Fluent, 2011):

$$C_D = \frac{24}{Re_D}\left(1 + 0.15 Re_D^{0.687}\right) \quad (3)$$

DEM accounts for the forces from the particle collisions and are determined as the overlap between pairs of spheres and between sphere and a boundary. The interactions were estimated by a Kelvin–Voigt model as shown in Fig. 2.

The normal component ($\underline{F}_N$) of the interactions $\underline{F}_{DEM}$ was estimated by (Crowe et al., 2012):

$$\underline{F}_N = \left[K\delta + \gamma\left(\underline{v}_{p-p'} \cdot \underline{e}_{p-p'}\right)\right]\underline{e}_{p-p'} \quad (4)$$

where K is the spring constant accounting for the elastic effect of the interactions between the spheres p and p', δ is the overlap between the spheres p and p', γ is the damping coefficient, $\underline{v}_{p-p'}$ is the relative velocity between the spheres p and p' and $\underline{e}_{p-p'}$ is the unit vector between spheres p and p'.

Parameters of Eq. (4) are determined by (Crowe et al., 2012):

$$\underline{e}_{p-p'} = \frac{\left(\underline{r}_p - \underline{r}_{p'}\right)}{|\underline{r}_p - \underline{r}_{p'}|} \tag{5}$$

$$\delta = |\underline{r}_p - \underline{r}_{p'}| - \left(R_p + R_{p'}\right) \tag{6}$$

$$\underline{v}_{p-p'} = \underline{v}_p - \underline{v}_{p'} \tag{7}$$

$$\gamma = -2\frac{m_{p-p'}\ln(\eta)}{t_{coll}} \tag{8}$$

$$m_{p-p'} = \frac{m_p m_{p'}}{m_p + m_{p'}} \tag{9}$$

$$t_{coll} = f_{loss}\sqrt{\frac{m_{p-p'}}{K}} \tag{10}$$

$$f_{loss} = \sqrt{\pi^2 + \ln^2(\eta)} \tag{11}$$

where $\underline{r}_i$ is the position vector of sphere i, R_i is the radius of sphere i, $m_{p-p'}$ is the reduced mass, m_i is the mass of sphere i, t_{coll} is the collision time scale, f_{loss} is a loss factor and η is a coefficient of restitution. It is important to mention that $0 < \eta \leq 1$ and that the damping coefficient is $\gamma \geq 0\,s^{-1}$ (Fluent, 2011; Crowe et al., 2012).

The tangential component ($\underline{F}_T$) of the interactions $\underline{F}_{DEM}$ was estimated by:

$$\underline{F}_T = \mu_{friction}\underline{F}_N \tag{12}$$

where $\mu_{friction}$ is the friction coefficient between spheres p and p'. The direction of $\underline{F}_T$ is opposite to the relative tangential motion.

The friction coefficient is a function of the tangential component ($v_{p-p',T}$) of the relative velocity vector between spheres ($\underline{v}_{p-p'}$). This parameter can be determined experimentally (Crowe et al., 2012). Specifically, Fluent (2011) calculates $\mu_{friction}$ as follows:

For $v_{p-p',T} \leq v_{glide}$

$$\mu = \mu_{stick} + \left(\mu_{stick} - \mu_{glide}\right)\left(\frac{v_{p-p',T}}{v_{glide}} - 2.0\right)\left(\frac{v_{p-p',T}}{v_{glide}}\right) \tag{13}$$

For $v_{glide} < v_{p-p',T} \leq v_{limit}$

$$\mu = \mu_{glide} \tag{14}$$

For $v_{p-p',T} > v_{limit}$

$$v_{ratio} = \frac{\left(v_{p-p'} - v_{limit}\right)}{s_{limit}} \tag{15}$$

$$\mu_{ratio} = \frac{\mu_{glide}}{\mu_{limit}} \tag{16}$$

$$\mu = \frac{(1.0 + v_{ratio})}{(1.0 + \mu_{ratio}v_{ratio})} \tag{17}$$

where μ_{stick} is the sticking friction coefficient, μ_{glide} is the gliding friction coefficient, μ_{limit} is the high velocity limit friction coefficient, v_{glide} is the gliding velocity, v_{limit} is the limit velocity, and s_{limit} is a parameter determining how fast μ approaches μ_{limit}.

For applying DEM, values of K, η, μ_{stick}, μ_{glide}, μ_{limit}, v_{glide}, v_{limit}, and s_{limit} are necessary. The values $\mu_{stick} = 0.5$, $\mu_{glide} = 0.2$, $\mu_{limit} = 0.1$, $v_{glide} = 1\,m\,s^{-1}$, $v_{limit} = 10\,m\,s^{-1}$ and $s_{limit} = 100\,s\,m^{-1}$ were suggested as default values in the software used. In the case of the spring constant, $K = 10{,}000\,s^{-2}$ was assumed. This value was chosen by trial and error following a practical guide of Fluent (2011) where it was suggested that K values should not be too low because spheres could overlapped or too high because the interaction would be too fast and the simulation time should be too small. Coefficients of restitution were determined as explained later. It is important to mention that a *Hertzian contact theory* (*i.e.* $\delta^{3/2}$ in Eq. (4)) can also be considered to estimate interactions in collisions but for the sake of simplicity only the linear relationship proposed in Eq. (4) is used (Crowe et al., 2012).

The energy transfer between the refrigerating medium and spheres was estimated by (Fluent, 2011; Crowe et al., 2012):

$$Nu_D = 2 + \left(0.4Re_D^{1/2} + 0.06Re_D^{2/3}\right)Pr^{0.4}\left(\frac{\mu}{\mu_s}\right)^{1/4} \tag{18}$$

where Nu_D is the Nusselt number based on the sphere diameter (h_cD/k), Re_D is the Reynold number ($\rho D v_{slip}/\mu$), Pr is the Prandtl number ($Cp\mu/k$), μ is the fluid viscosity at the refrigerating medium temperature, μ_s is the fluid viscosity at the sphere surface temperature, h_c is the surface heat transfer coefficient, k is the fluid thermal conductivity, and Cp is the fluid heat capacity. Eq. (18) is valid for $0.7 < Pr < 380$, $3.5 < Re_D < 8 \times 10^4$ and $1 < \mu/\mu_s < 3.2$ (Perry and Green, 2008). It is worth mentioning that the value μ_s was calculated at an average temperature of the refrigerating medium and initial sphere surface temperatures.

The mass transfer coefficient (k_c) was estimated through the surface heat transfer coefficient and the Chilton–Colburn analogy (Peralta et al., 2012).

Computational domain and conditions of the simulations

The computational domain was similar to the physical domain showed in Fig. 1. The fluid exit was considered as a 6-mm width slit placed at the top of the cylindrical wall of the domain. The solid walls were assumed to be adiabatic and the pressure 0.1 MPa. A 1/7th power velocity profile was used in the orifices because a fully turbulent liquid-jet was assumed. A turbulence intensity of 5% was assumed at the exit of orifices (Peralta et al., 2010). The 13 spheres of 10-mm diameter were initially placed in a regularly spaced squared array. The geometrical centers of spheres were separated a distance $L = 20$ mm. The distance between the stagnation point of spheres and the orifice plate was 30 mm.

The computational domain was discretized by using a mesh composed by tetrahedral. The density of the mesh was higher in the zone near the orifices. Each condition was simulated up to 8 s. During the first 3 s, the fluid was simulated to reach a quasi-steady state and the next 5 s the spheres and interactions were simulated.

The balance equations (Navier–Stokes, DPM, DEM) were solved by using the commercial CFD software ANSYS-ICEM-CFD 14.1 and ANSYS-FLUENT 14.1 (Ansys Inc., Canonsburg, USA). Simulations were carried out using a PC Intel core i7

3930 of 3.2 GHz with 16 GB of RAM (DDR3 1600 MHz). Each simulation took approximately 90 h to converge.

2.2.2. *Heat and mass transfer in the food sample*

Heat and mass transfer inside the food sample were estimated using the mathematical model developed by Zorrilla and Rubiolo (2005a,b) and extended to spherical geometries by Peralta et al. (2012). The computational domain was 10-mm diameter spheres. Parameters of potato necessary to complete the model were obtained from Peralta et al. (2012).

Computational domain and conditions of the simulations

The computational domain was a sphere of 10-mm diameter. The balances were applied in spherical coordinates taking into account radial dimension in transient conditions and were solved using a finite difference method. The discretization of the food domain was performed by using 30 segments in r direction. A logarithmic discretization were used in r direction due to the main changes occur near the interface food–fluid (Peralta et al., 2012). The numerical scheme was implemented in a computer program using Fortran language (Intel Fortran Composer XE 2013, Santa Clara, USA) and it was solved using a PC Intel core i7 3930 of 3.2 GHz with 16 Gb RAM (DDR3 1600 MHz). Each condition was simulated up to 600 s and took approximately 3 min to converge.

2.2.3. *Connection between the fluid and food domains*

The balances were solved by decoupling the momentum from energy and mass transfer. This procedure was carried out taking into account the difference in orders of magnitude between the transfer rate of momentum and energy or mass (Peralta et al., 2012).

The surface heat transfer coefficient ($\langle\langle h_c\rangle\rangle$) was used as the variable that carries the information of the transfer phenomena between the refrigerating medium and the food sample. Surface heat transfer coefficients obtained with Eq. (18) changing with time were used to calculate the average value as explained later.

2.3. *Measurement of DEM input parameters*

The coefficients of restitution are the main parameters necessary to apply DEM. There are two kind of restitution coefficients, a restitution coefficient related to the sphere-wall interactions (η_w) and a restitution coefficient related to the sphere–sphere interactions (η_p).

2.3.1. *Coefficient of restitution for sphere–wall interactions*

For the determination of η_w, drop tests similar to those described by Kharaz and Gorham (2000), Dong and Moys (2003, 2006), Chung (2006), Wong et al. (2009), and González-Montellano et al. (2012) were used. Briefly, potato spheres of 20-mm diameter were released onto a horizontal flat steel surface at a height $h_0 = 5$, 10, 15, 20, and 25 cm. The sphere fell freely until impacting the surface and bounced to a height h_1. The heights were determined by images captured with a digital camera (Noganet, Buenos Aires, Argentina) of 5 MP running at 25 frames per second with a resolution of 640 × 480. A 1-mm scale in the background was used as height reference. Images were recorded with *GTK UV video viewer* software and processed with *ffmpeg* software. Assays were replicated 20 times. The measurement system was validated determining the coefficient of restitution η_w for a polypropylene sphere of 20-mm diameter. In that case, assays were replicated 5 times. Assuming that the energy is conserved before and after impact, η_w can be calculated by (González-Montellano et al., 2012)

$$\eta_w = \sqrt{\frac{h_1}{h_0}} \tag{19}$$

2.3.2. *Coefficient of restitution for sphere–sphere interactions*

For the determination of η_p, impact tests similar to those described by Wong et al. (2007) and González-Montellano et al. (2012) were used. Briefly, 2 potato spheres of 20-mm diameter were suspended and aligned using cotton strings and hanging them on a horizontal bar to carry out a pendulum test (or collision between spheres). One of the spheres (sphere 1) was moved laterally to a height $h_0 = 5$, 10, 15 or 20 cm and it was released to impact against sphere 2. Spheres 1 and 2 reached heights h_1 and h_2, respectively. The heights were determined by image analysis as described before. Assays were replicated 10 times. The measurement system was validated determining the coefficient of restitution η_p for polypropylene spheres of 20-mm diameter. In this case, assays were replicated 4 times. Assuming that the energy is conserved before and after impact, η_p can be calculated by (González-Montellano et al., 2012)

$$\eta_p = \frac{\sqrt{h_2} - \sqrt{h_1}}{\sqrt{h_0}} \tag{20}$$

2.4. *Variables analyzed*

Representative variables were conveniently selected to study the transport phenomena of the system studied: the average velocity of spheres ($\langle v_p\rangle$), the average relative fluid velocity ($\langle v_{slip}\rangle$), the volume-averaged turbulence intensity ($\langle Tu\rangle$), the volume-averaged surface heat transfer coefficient ($\langle h_c\rangle$), and the time-averaged surface heat transfer coefficient ($\langle\langle h_c\rangle\rangle$).

$$\langle v_p\rangle = \frac{1}{V_T}\int_{V_T} |\underline{v}_p| dV \tag{21}$$

$$\langle v_{slip}\rangle = \frac{1}{V_T}\int_{V_T} v_{slip} dV = \frac{1}{V_T}\int_{V_T} |\underline{v}_p - \underline{v}_f| dV \tag{22}$$

$$\langle Tu\rangle = \frac{1}{V_T}\int_{V_T} Tu dV \tag{23}$$

$$\langle h_c\rangle = \frac{1}{V_T}\int_{V_T} h_c dV \tag{24}$$

$$\langle\langle h_c\rangle\rangle = \frac{1}{t_{Res}}\int_{t_{Res}} \langle h_c\rangle dt \tag{25}$$

where $\underline{v}_p$ is the velocity of sphere p, $|\underline{v}_p|$ is the magnitude of $\underline{v}_p$, $\underline{v}_f$ is the fluid velocity, v_{slip} is the magnitude of the sphere velocity relative to the fluid velocity, Tu is the local turbulence intensity, h_c is the surface heat transfer coefficient of each sphere, V_T is the total domain volume and t_{Res} is the total residence time of the spheres in the domain.

It is important to mention that, as implied by Fikiin (2008), one of the features of HF is that the frozen products have an attractive appearance and tend to do not stick together due to the fluidized nature (*i.e.* stochastic) of the process. Therefore, a correct description of the product dispersion level based

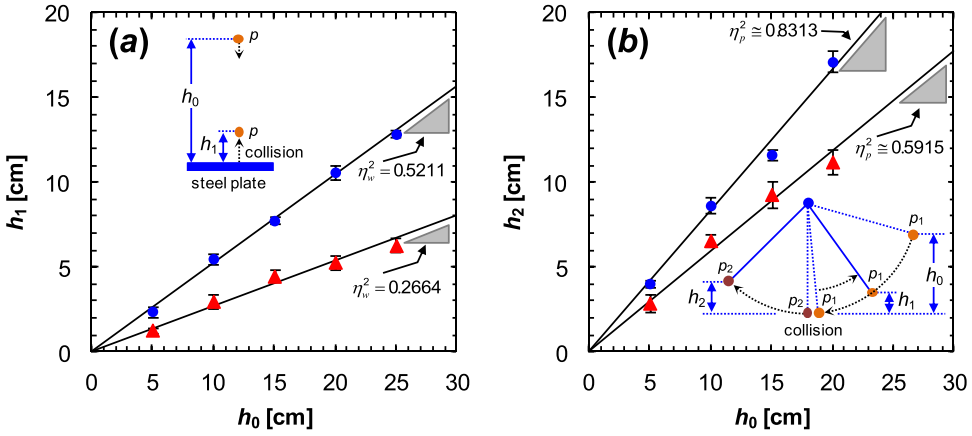

Fig. 3 – Experimental data to determine the coefficients of restitution: (a) for sphere–wall interactions, (b) for sphere–sphere interactions. (●) Polypropylene, (▲) potato.

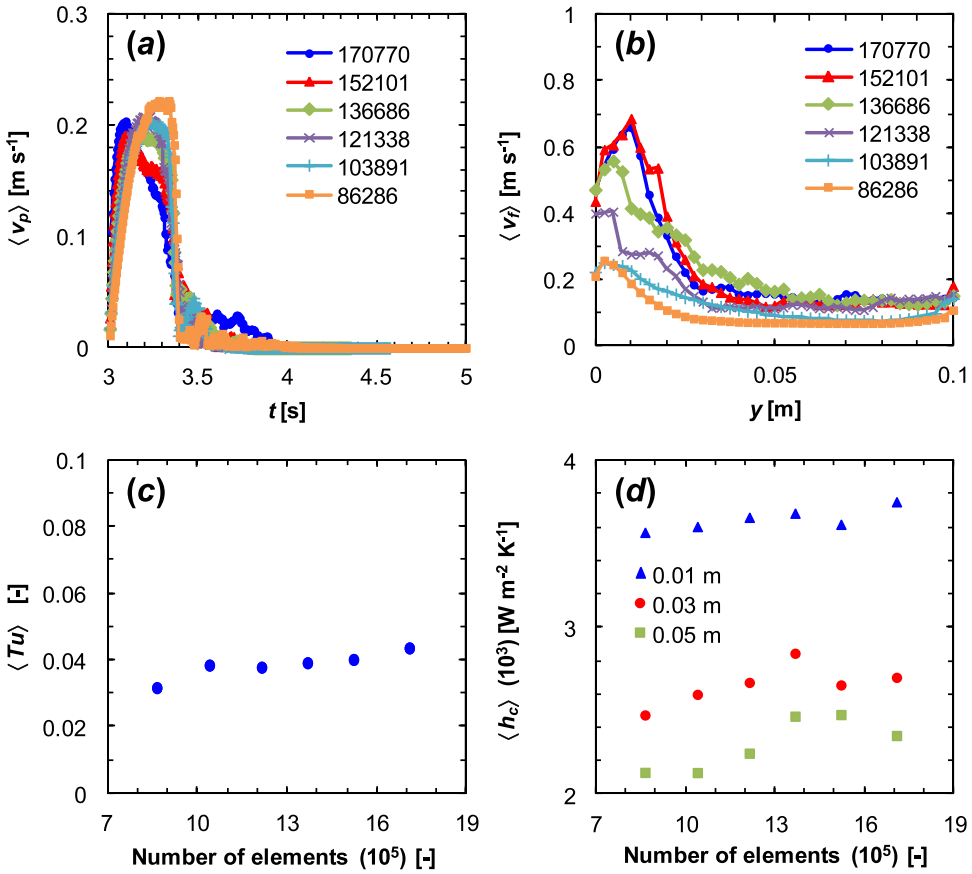

Fig. 4 – Mesh independence. Values of (a) $\langle v_p \rangle$ as a function of simulation time, (b) $\langle v_f \rangle$ as a function of axial position, (c) $\langle Tu \rangle$, (d) $\langle h_c \rangle$, considering different mesh composition.

on the operative variables is crucial to control the fluidization process and to ensure the quality of the products. In general, the fluidization level (*i.e.* dispersion level of the particles) in fluidized beds composed by a large number of particles is correlated to the pressure drop through the bed (Smith, 2007). In this case (*i.e.* small number of particles), as the position of all particles is relatively easy to compute, the dispersion level can be calculated directly. Then, a dispersion level of the spheres in the domain was estimated using a dimensionless average minimum distance ($\langle d \rangle_t$) (Clark and Evans, 1954; Illian et al., 2008; O'sullivan and Unwin, 2010):

$$\langle d \rangle_t = \frac{\langle d_{min} \rangle_t}{\langle d_{min} \rangle_0} = \frac{1}{\langle d_{min} \rangle_0} \sum_{i=1}^{n} \min_{i \neq j} \left\{ d_{ij} \right\}_{j=1}^{n} \quad (26)$$

where $\min_{i \neq j} \left\{ d_{ij} \right\}_{j=1}^{n}$ is the minimum value of d_{ij} in the Euclidean distances of the geometrical centers $\left\{ d_{i1}, d_{i2}, d_{i3}, \ldots, d_{in} \right\}$ excluding the distance $d_{i=j}$.

It should be clear that for a large number of particles producing a more dense bed, the pressure drop through the bed would be a more sensitive parameter to characterize the fluidization process.

2.5. *Model validation*

The mathematical model used in this work was partially validated comparing results with those obtained by Nouri et al. (2014) who studied a sphere falling vertically in water under

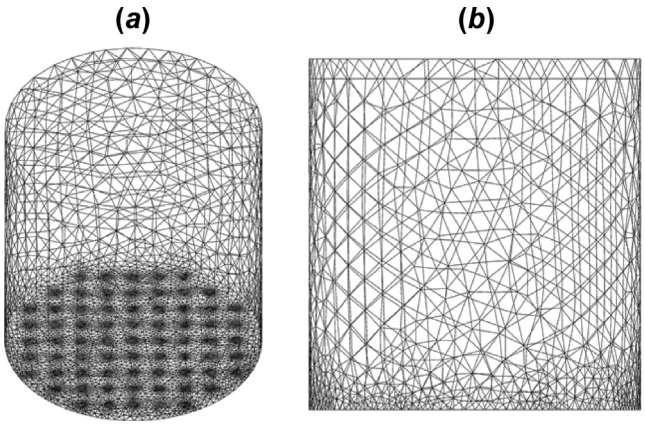

Fig. 5 – Views of mesh used for the simulations: (a) volume view, (b) lateral view.

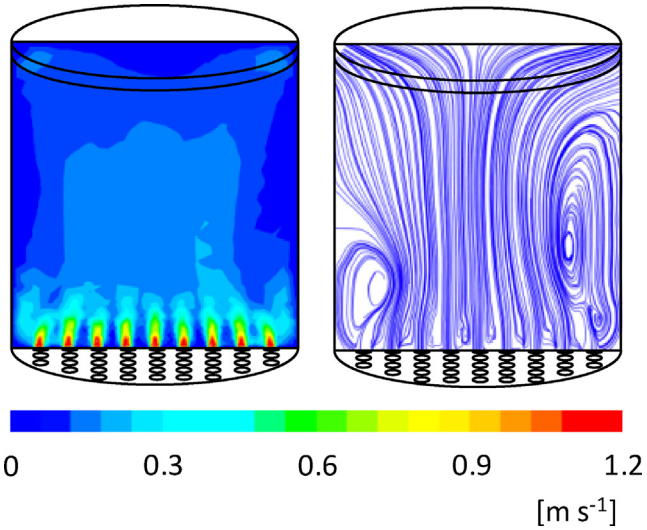

Fig. 7 – Velocity contours and streamlines for the study case and t = 3 s.

the influence of gravity and with those obtained by Belis et al. (2015) who study a similar hydrofluidization system.

3. Results and discussion

3.1. *Coefficients of restitution*

Fig. 3 shows the experimental results obtained and the corresponding regression equations related to Eqs. (19) and (20) for the materials studied. It is worth mentioning that $h_1 \cong 0$ in Eq. (20) for the cases studied. The coefficients of restitution for polypropylene were $\eta_w = 0.72$ and $\eta_p = 0.91$ that are in the order of magnitude of values reported in literature (Constantinides et al., 2008). The coefficients of restitution for potato were $\eta_w = 0.52$ and $\eta_p = 0.77$.

3.2. *Mesh independence test*

The mesh independence was tested using the local values of $\langle v_p \rangle$, $\langle v_f \rangle$ at 3 s, $\langle Tu \rangle$ at 3 s, and $\langle h_c \rangle$ at 3 s. It is worth mentioning that $\langle v_f \rangle$ is the area-averaged fluid velocity at a surface perpendicular to y-axis at a position y ($A_y^{-1} \int_{A_y} |\underline{v}_f| dA$). Different numbers of elements were evaluated (from 86,296 to 170,770 tetrahedra). It was also taken into account that the element size be equal or bigger than the spheres to minimize convergence problems (Fluent, 2011). Fig. 4 shows the variables analyzed for different meshes studied. A mesh composed of 170,770 elements was used for simulations (Fig. 5).

3.3. *Model validation*

Nouri et al. (2014) studied the unsteady settling behavior of solid spheres falling in water and developed an analytical method to evaluate sedimentation. Fig. 6a shows the values of the sphere velocity magnitude ($|\underline{v}_p|$) and the sphere position (y_p) as function of time for a sphere of 10-mm diameter released at $H_0 = 100$ mm and falling in water. Two values of sphere density (ρ_p) in the order of magnitude of values for potato were considered. The values obtained with the model proposed by Nouri et al. (2014) and those obtained with the model proposed in this work showed excellent agreement (average percentage error less than 1.5%).

Belis et al. (2015) studied the transport phenomena in a hydrofluidization system with several static spheres. Fig. 6b shows the surface heat transfer coefficients obtained by Belis et al. (2015) and those obtained in this work. The conditions selected for comparison consisted in 13 spheres of 20-mm diameter at the initial time, with a distance between the geometrical centers of 20 mm, and with the distance between the plane of the orifice plate and the stagnation point of the spheres $H_0 = 10$ mm and $H_0 = 50$ mm. Different area averaged fluid velocity at the orifices allowed comparing 8 different conditions that produced surface heat transfer coefficients in the range of $1000\ W\ m^{-2}\ K^{-1} < h_c < 5000\ W\ m^{-2}\ K^{-1}$. An average

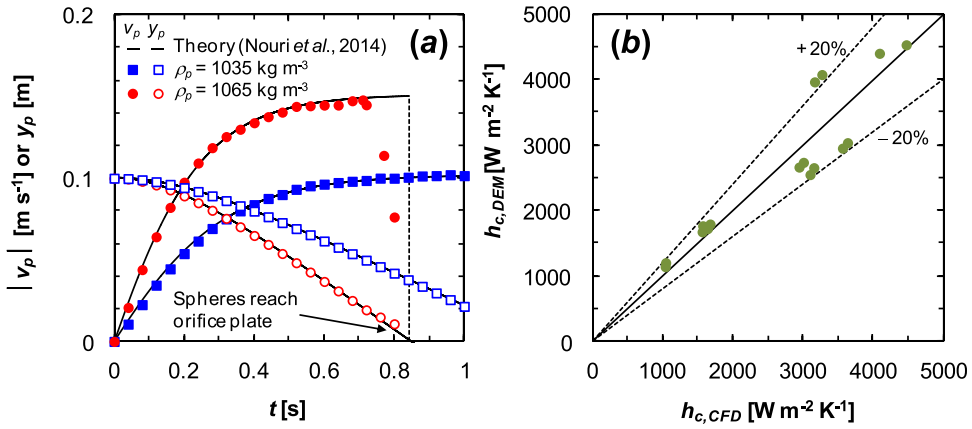

Fig. 6 – Model validation. Comparison with: (a) values of $|\underline{v}_p|$ and y_p obtained by Nouri et al. (2014) for a sphere falling in water, and (b) values of h_c obtained by Belis et al. (2015) for a similar hydrofluidization system.

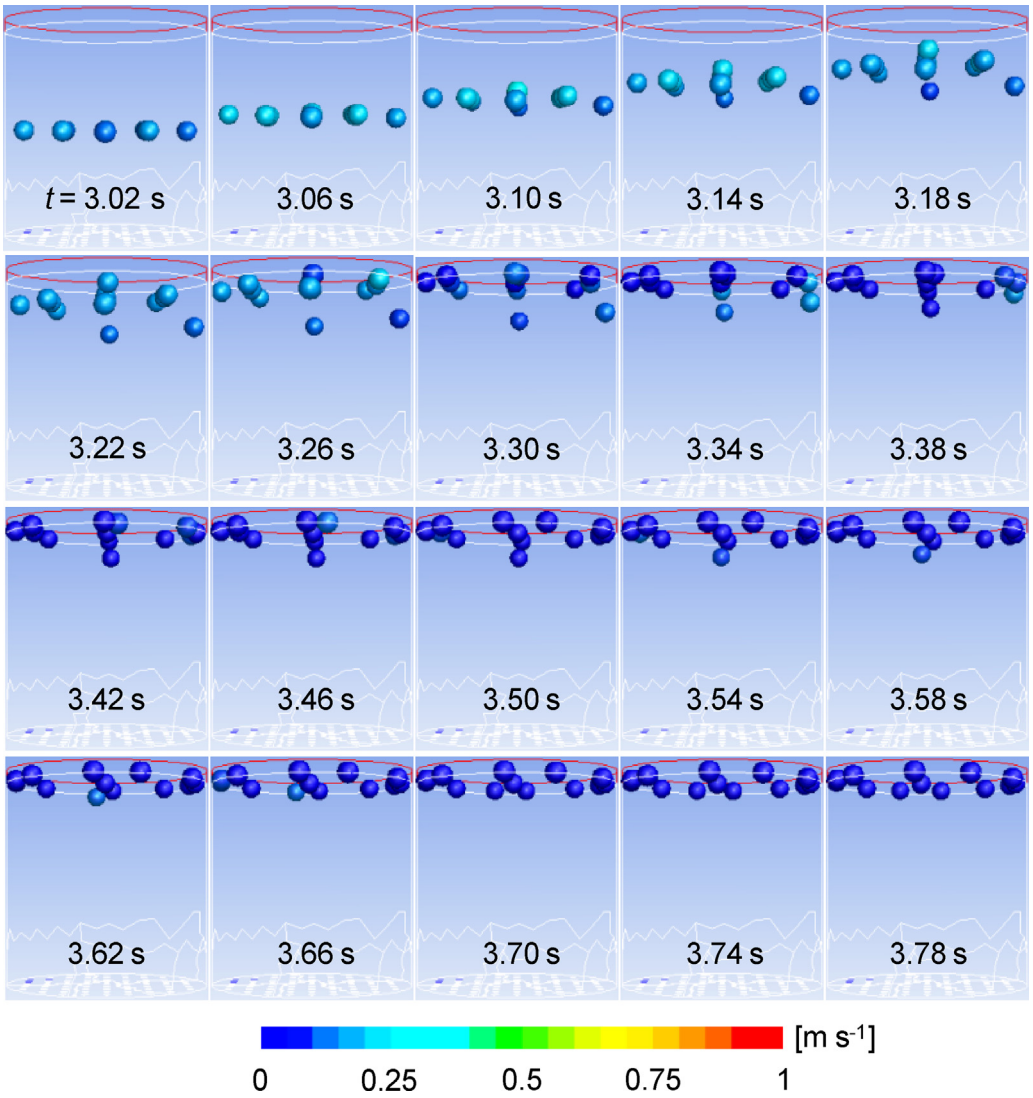

Fig. 8 – Behavior of spheres after injection for the study case. Color of spheres represents the velocity of spheres.

percentage error less than 13% indicated a good agreement between the models compared.

3.4. *Velocity contours and streamlines*

Velocity contours with their respective streamlines are shown in Fig. 7. It is worth mentioning that an arbitrary cut plane is shown to represent the 3D information more easily. The flow field shown corresponds to $t = 3$ s (immediately before injection of spheres).

In general, the velocity contours presented similar features to those observed by Belis et al. (2015) with high local velocities close to the zones where jets are developed. It can be observed interaction zones among jets and recirculation zones. Due to the number of orifices, less perturbed jet cores, higher local velocities and less perturbed streamlines are observed close to the domain axis. It is important to mention that periodic eddies form and dissipate in the domain.

3.5. *Behavior of spheres in the fluid domain*

Fig. 8 shows the behavior and the trajectories of the spheres after injection as a function of time. It can be observed that spheres continuously ascend according to their initial position. The spheres did not perturb the fluid field. The fastest spheres were those initially placed at the axis of the domain and the slowest were those ascending near the domain walls. All the spheres finished their ascending at the liquid–air interface approximately 1 s after being injected, and with similar initial distribution.

The volume-averaged velocity of spheres ($\langle v_p \rangle$) as a function of time is shown in Fig. 9a. At the beginning, $\langle v_p \rangle$ increases to a maximum due to the initial contact of the spheres with the refrigerating medium. Then, an approximately plateau region was observed. Finally, a subsequent reduction to zero velocity values was obtained when the spheres reached the liquid–air interface.

The volume-averaged relative fluid velocity ($\langle v_{slip} \rangle$) as a function of time is shown in Fig. 9b. An initial velocity equal to the fluid velocity was observed at the injection point of the spheres due to the zero initial velocity of the spheres. A subsequent decrease was observed due to an initial velocity increment of the spheres and a slight decrease of the fluid velocity detected by the spheres as they ascend inside the domain. Then, a minimum is obtained when $\langle v_p \rangle$ and the fluid velocity are equaled. A zero value is obtained at this point but is not shown in Fig. 9b due to the time discretization used. Then, a second maximum is observed when spheres reached their maximum $\langle v_p \rangle$, followed by a slight decrease or plateau according to $\langle v_p \rangle$ profiles (Fig. 9a) and small values of fluid

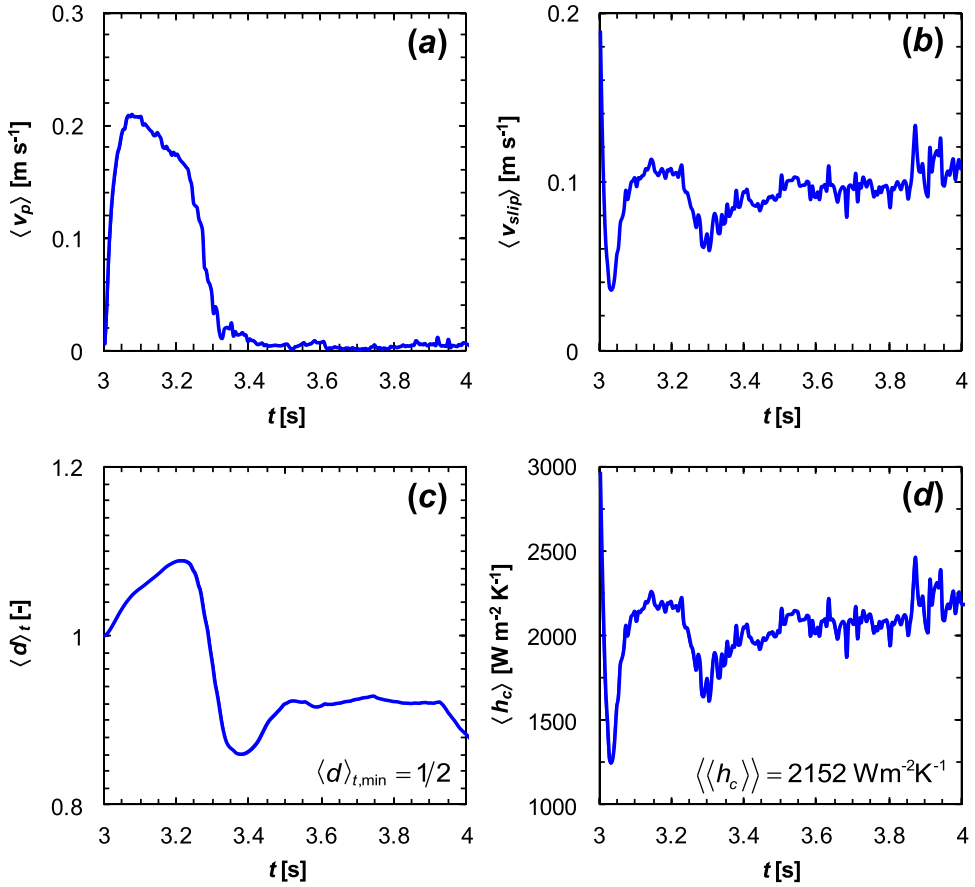

Fig. 9 – Average values (a) $\langle v_p \rangle$, (b) $\langle v_{slip} \rangle$, (c) $\langle d \rangle_t$, and (d) $\langle h_c \rangle$ as a function of time after injection of spheres in the fluid domain.

velocity. Finally, a value of $\langle v_{slip} \rangle$ equal to the fluid velocity is obtained due to the spheres reached the liquid–air interface and $\langle v_p \rangle = 0$.

The dispersion level of the spheres measured through the average minimum distance ($\langle \langle d \rangle_t \rangle$) as function of time is shown in Fig. 9c. The values of $\langle d \rangle_t$ increase until reaching a maximum for $3.2\,s < t < 3.4\,s$. The dispersion of spheres can be related to the interaction of spheres with the fluid, between them and with the walls. Then, a decrease of $\langle d \rangle_t$ is observed due to spheres are grouped together until reached the liquid–air interface. However, spheres did not reach the value $\langle d \rangle_{t,min} = 1/2$ during the period of time studied (*i.e.* spheres touched each other).

3.6. *Surface heat transfer coefficient*

The profile of the volume-averaged surface heat transfer coefficient ($\langle h_c \rangle$) as a function of time is shown in Fig. 9d. Values are shown in the range of $3\,s < t < 4\,s$ and were in the range of $800\,W\,m^{-2}\,K^{-1} < \langle h_c \rangle < 4000\,W\,m^{-2}\,K^{-1}$. The behavior observed is similar to that observed for $\langle v_{slip} \rangle$ (Fig. 9b) due to the relationship of these variables through Eq. (18). The time-averaged surface heat transfer coefficient $\langle \langle h_c \rangle \rangle$ for $t_{Res} = t_f - t_0 = 5\,s$ was $2152\,W\,m^{-2}\,K^{-1}$.

3.7. *Heat and mass transfer in the food domain*

The mass and heat transfer in the food domain can be studied through the average NaCl concentration (C_{NaCl}) and through the temperature at the geometric center of the spheres (T_c), respectively (Peralta et al., 2012). Fig. 10 shows the progressive approach to represent the physical scenario of HF through the models developed by Peralta et al. (2012), Belis et al. (2015) and the one developed in this work. The regions of expected changes in the results considering the approach proposed in this work are also shown. The comparison is mainly based on the different kind of heat transfer coefficient used to connect the fluid and food domain information.

4. Conclusions

Coupled CFD–DPM–DEM simulations were used to study a hydrofluidization system with moving food spheres and multiple jets. This approach gives a more realistic description of the system. DPM allows following the trajectory of spheres while DEM allows obtaining the sphere–sphere and sphere–walls interactions. Restitution coefficients are important parameters for DEM and were determined for the case studied. Model proposed was partially validated with information obtained from literature for similar systems and good agreement was found. The description of the case studied through the representative variables allows improving the understanding and representation of the complex system studied. The surface heat transfer coefficients obtained were more realistic than those obtained with previous models for hydrofluidization systems.

This study shows that CFD–DPM–DEM can be a powerful tool to simulate food processing systems, where a certain amount of small or large food particles move within the fluid domain, with minimum computational requirements compared to approaches where fluid to particle interactions with moving meshes are used. Further validation studies are nec-

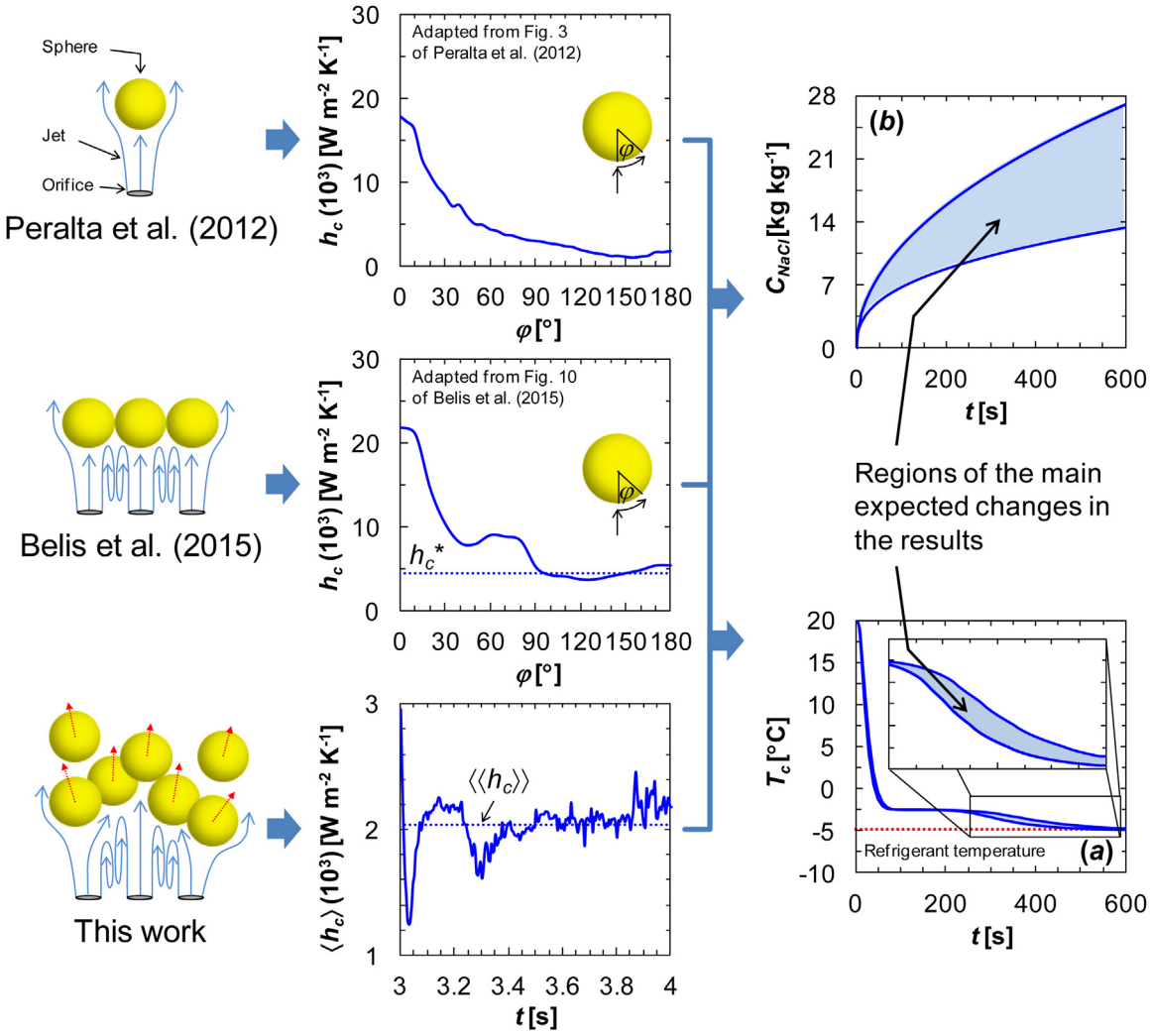

Fig. 10 – Schematic comparison of models proposed by Peralta et al. (2012), Belis et al. (2015) and in this work. Expected changes in the results when temperature at the geometric center of spheres and average NaCl concentration are predicted.

essary to reinforce the knowledge of the model capability to estimate the main variables involved.

Acknowledgments

This research was supported partially by Universidad Nacional del Litoral (project CAI+D 501 201101 00031 LI) (Santa Fe, Argentina), Consejo Nacional de Investigaciones Científicas y Técnicas (Argentina), and Agencia Nacional de Promoción Científica y Tecnológica (projects ANPCyT: 2011-182 and 2012-1413) (Argentina).

References

Belis, E.E., Zorrilla, S.E., Peralta, J.M., 2015. Effect of the number of orifices and operative variables on the heat and mass transfer in a hydrofluidization system with static spheres. J. Food Eng. 153, 96–107, http://dx.doi.org/10.1016/j.jfoodeng.2014.12.016.

Chung, Y.-C., 2006. Discrete Element Modelling and Experimental Validation of a Granular Solid Subject to Different Loading Conditions (Ph.D.). The University of Edinburgh, Edinburgh, Scotland.

Clark, P.J., Evans, F.C., 1954. Distance to nearest neighbor as a measure of spatial relationships in populations. Ecology 35, 445–453, http://dx.doi.org/10.2307/1931034.

Constantinides, G., Tweedie, C., Holbrook, D., Barragan, P., Smith, J., Van Vliet, K., 2008. Quantifying deformation and energy dissipation of polymeric surfaces under localized impact. Mater. Sci. Eng. A 489, 403–412, http://dx.doi.org/10.1016/j.msea.2007.12.044.

Crowe, C.T., Schwarzkopf, J.D., Sommerfeld, M., Tsuji, Y., 2012. Multiphase Flows with Droplets and Particles, 2nd ed. CRC Press, Boca Raton, FL.

Cundall, P.A., Strack, O.D.L., 1979. A discrete numerical model for granular assemblies. Géotechnique 29, 47–65, http://dx.doi.org/10.1680/geot.1979.29.1.47.

Dong, H., Moys, M.H., 2003. Measurement of impact behaviour between balls and walls in grinding mills. Miner. Eng. 16, 543–550, http://dx.doi.org/10.1016/S0892-6875(03)00057-8.

Dong, H., Moys, M.H., 2006. Experimental study of oblique impacts with initial spin. Powder Technol. 161, 22–31, http://dx.doi.org/10.1016/j.powtec.2005.05.046.

Fikiin, A.G., 1992. New method and fluidized water system for intensive chilling and freezing of fish. Food Control 3, 153–160, http://dx.doi.org/10.1016/0956-7135(92)90100-O.

Fikiin, K., 2003. Novelties of Food Freezing Research in Europe and Beyond. Flair-Flow Europe Synthetic Brochure for SMEs No. 10. Institut National de la Recherche Agronomique, Paris, France.

Fikiin, K., 2008. Emerging and novel freezing processes. In: Evans, J.A. (Ed.), Frozen Food Science and Technology. Blackwell Publishing Ltd., Oxford, UK, pp. 101–123.

Fikiin, K., Fikiin, A., 1998. Individual quick freezing of foods by hydrofluidisation and pumpable ice slurries. In: Fikiin, K. (Ed.), IIR Proceedings Series Refrigeration Science and Technology. Presented at the International Conference on Advances in the Refrigeration Systems, Food Technologies and Cold. Sofia, Bulgaria, pp. 319–326, http://dx.doi.org/10.13140/RG.2.1.3901.1283/1.

Fluent, 2011. ANSYS FLUENT Theory Guide Release 14.0. ANSYS, Inc., Canonsburg, PA.
Fries, L., Antonyuk, S., Heinrich, S., Palzer, S., 2011. DEM–CFD modeling of a fluidized bed spray granulator. Chem. Eng. Sci. 66, 2340–2355, http://dx.doi.org/10.1016/j.ces.2011.02.038.
Fryer, P.J., Porras-Parral, G., Bakalis, S., 2011. Multiphysics modeling of Ohmic heating. In: Knoerzer, K., Juliano, P., Roupas, P., Versteeg, C. (Eds.), Innovative Food Processing Technologies: Advances in Multiphysics Simulation. Blackwell Publishing Ltd., Oxford, UK, pp. 155–169.
Gidaspow, D., 1994. Multiphase Flow and Fluidization: Continuum and Kinetic Theory Descriptions. Academic Press, Boston, MA.
González-Montellano, C., Fuentes, J.M., Ayuga-Téllez, E., Ayuga, F., 2012. Determination of the mechanical properties of maize grains and olives required for use in DEM simulations. J. Food Eng. 111, 553–562, http://dx.doi.org/10.1016/j.jfoodeng.2012.03.017.
Illian, J., Penttinen, A., Stoyan, H., Stoyan, D., 2008. Statistical Analysis and Modelling of Spatial Point Patterns. John Wiley & Sons, Chichester, England.
Kharaz, A.H., Gorham, D.A., 2000. A study of the restitution coefficient in elastic-plastic impact. Philos. Mag. Lett. 80, 549–559, http://dx.doi.org/10.1080/09500830050110486.
Kloss, C., Goniva, C., Hager, A., Amberger, S., Pirker, S., 2012. Models, algorithms and validation for opensource DEM and CFD–DEM. Prog. Comput. Fluid Dyn. Int. J. 12, 140, http://dx.doi.org/10.1504/PCFD.2012.047457.
Norton, T., Sun, D.-W., 2007. An overview of CFD applications in the food industry. In: Sun, D.-W. (Ed.), Computational Fluid Dynamics in Food Processing. CRC Press, Boca Raton, FL, pp. 1–41.
Norton, T., Tiwari, B., 2014. Computational fluid dynamics in food processing. In: Sahu, J. (Ed.), Introduction to Advanced Food Process Engineering. CRC Press, Boca Raton, FL, pp. 343–374.
Nouri, R., Ganji, D.D., Hatami, M., 2014. Unsteady sedimentation analysis of spherical particles in Newtonian fluid media using analytical methods. Propuls. Power Res. 3, 96–105, http://dx.doi.org/10.1016/j.jppr.2014.05.003.
O'sullivan, D., Unwin, D., 2010. Geographic Information Analysis, 2nd ed. John Wiley & Sons, Hoboken, NJ.
Peralta, J.M., Rubiolo, A.C., Zorrilla, S.E., 2007. Prediction of heat capacity, density and freezing point of liquid refrigerant solutions using an excess Gibbs energy model. J. Food Eng. 82, 548–558, http://dx.doi.org/10.1016/j.jfoodeng.2007.03.010.
Peralta, J.M., Rubiolo, A.C., Zorrilla, S.E., 2009. Design and construction of a hydrofluidization system. Study of the heat transfer on a stationary sphere. J. Food Eng. 90, 358–364, http://dx.doi.org/10.1016/j.jfoodeng.2008.07.004.
Peralta, J.M., Rubiolo, A.C., Zorrilla, S.E., 2010. Mathematical modeling of the heat transfer and flow field of liquid refrigerants in a hydrofluidization system with a stationary sphere. J. Food Eng. 99, 303–313, http://dx.doi.org/10.1016/j.jfoodeng.2010.03.003.
Peralta, J.M., Rubiolo, A.C., Zorrilla, S.E., 2012. Mathematical modeling of the heat and mass transfer in a stationary potato sphere impinged by a single round liquid jet in a hydrofluidization system. J. Food Eng. 109, 501–512, http://dx.doi.org/10.1016/j.jfoodeng.2011.10.032.
Perry, R.H., Green, D.W., 2008. Perry's Chemical Engineers' Handbook, 8th ed. McGraw-Hill, New York, NY.
Ren, B., Zhong, W., Chen, Y., Chen, X., Jin, B., Yuan, Z., Lu, Y., 2012. CFD–DEM simulation of spouting of corn-shaped particles. Particuology 10, 562–572, http://dx.doi.org/10.1016/j.partic.2012.03.011.
Schulze, S., Schmidt, R., Nikrityuk, P.A., 2014. Modeling of moving particles: review of basic concepts and models. In: Nikrityuk, P.A., Meyer, B. (Eds.), Gasification Processes. Wiley-VCH Verlag GmbH & Co. KGaA, Weinheim, Germany, pp. 43–72.
Smith, P.G., 2007. Applications of Fluidisation in Food Processing, 1st ed. Blackwell Science, Oxford, UK.
Stankiewicz, A.I., Moulijn, J.A., 2004. Re-engineering the Chemical Processing Plant: Process Intensification, Chemical Industries. Marcel Dekker Inc., New York, NY.
Thornton, C., 2015. Granular Dynamics, Contact Mechanics and Particle System Simulations, Particle Technology Series. Springer International Publishing, Cham, Switzerland.
Tsotsas, E., Mujumdar, A.S., 2014. Modern Drying Technology. Vol. 5: Process Intensification. Wiley-VCH Verlag GmbH & Co. KGaA, Weinheim, Germany.
Verboven, P., Scheerlinck, N., Nicolaï, B.M., 2003. Surface heat transfer coefficients to stationary spherical particles in an experimental unit for hydrofluidisation freezing of individual foods. Int. J. Refrig. 26, 328–336, http://dx.doi.org/10.1016/S0140-7007(02)00110-X.
Wilcox, D.C., 2006. Turbulence Modeling for CFD, 3rd ed. DCW Industries, La Canada, CA.
Wong, C., Daniel, M., Rongong, J., 2007. Prediction of the amplitude dependent behaviour of particle dampers. In: 48th AIAA/ASME/ASCE/AHS/ASC Structures, Structural Dynamics, and Materials Conference, American Institute of Aeronautics and Astronautics, Honolulu, Hawaii, http://dx.doi.org/10.2514/6.2007-2043.
Wong, C.X., Daniel, M.C., Rongong, J.A., 2009. Energy dissipation prediction of particle dampers. J. Sound Vib. 319, 91–118, http://dx.doi.org/10.1016/j.jsv.2008.06.027.
Wu, C.L., Ayeni, O., Berrouk, A.S., Nandakumar, K., 2014. Parallel algorithms for CFD–DEM modeling of dense particulate flows. Chem. Eng. Sci. 118, 221–244, http://dx.doi.org/10.1016/j.ces.2014.07.043.
Wu, C.-Y., 2012. Discrete Element Modelling of Particulate Media, Special Publication. Royal Society of Chemistry, Cambridge, UK.
Zhang, L.-P., Zhang, J., Li, C.-H., Bao, J., 2014. Rheological characterization and CFD modeling of corn stover-water mixing system at high solids loading for dilute acid pretreatment. Biochem. Eng. J. 90, 324–332, http://dx.doi.org/10.1016/j.bej.2014.06.018.
Zorrilla, S.E., Rubiolo, A.C., 2005a. Mathematical modeling for immersion chilling and freezing of foods: part I: model development. J. Food Eng. 66, 329–338, http://dx.doi.org/10.1016/j.jfoodeng.2004.03.026.
Zorrilla, S.E., Rubiolo, A.C., 2005b. Mathematical modeling for immersion chilling and freezing of foods: part II: model solution. J. Food Eng. 66, 339–351, http://dx.doi.org/10.1016/j.jfoodeng.2004.03.027.